Irreversible Electroporation Ablation of Malignant Hepatic Tumors: Subacute and Follow-up CT Appearance of Ablation Zones

Marco Dollinger, MD, Ernst-Michael Jung, MD, Lukas Beyer, MD, Christoph Niessen, MD, Fabian Scheer, MD, René Müller-Wille, MD, Christian Stroszczynski, MD, and Philipp Wiggermann, MD

ABSTRACT

Purpose: To describe findings on contrast-enhanced computed tomography (CT) images of malignant hepatic tumors 24–72 hours after percutaneous ablation by irreversible electroporation (IRE) and at midterm follow-up.

Materials and Methods: Retrospective analysis of 52 malignant liver tumors—30 primary hepatic tumors and 22 hepatic metastases—in 34 patients (28 men and 6 women, mean age 64 y) treated by IRE ablation was performed. Ablation zones were evaluated by two examiners in a consensus reading by means of a dual-phase CT scan (consisting of a hepatic arterial and portal venous phase) performed 24–72 hours after IRE ablation and at follow-up.

Results: During the portal venous phase, ablation zones either were homogeneously hypoattenuating (n = 36) or contained heterogeneously isoattenuating or hyperattenuating (n = 16) foci, or both, in a hypoattenuating area. Of 52 lesions, 38 included gas pockets. Peripheral contrast enhancement of the ablation defect was evident in 23 tumors during the arterial phase and in 36 tumors during the portal venous phase. Four tumors showed intralesional abscesses after the intervention. At follow-up (mean, 4.7 mo), the mean volume of the ablation defects was reduced to 29% of their initial value.

Conclusions: Because normal findings on contrast-enhanced CT images after IRE ablation may be very similar to the typical characteristics of potential complications following ablation, such as liver abscesses, CT scans must be carefully analyzed to distinguish normal results after intervention from complications requiring further treatment.

ABBREVIATIONS

IRE = irreversible electroporation, MW = microwave

Irreversible electroporation (IRE) has emerged more recently as a novel, theoretically nonthermal ablative technique that disrupts the integrity of cell membranes, subsequently causing cell death by delivering a series of high-voltage electrical pulses of millisecond duration to the surrounding tissue (1–4). IRE is a new type of ablative procedure that is not based on thermal energy, but rather is based on electrical energy. IRE is currently being investigated in both animal and human studies. The results of animal studies indicate that blood vessels, bile ducts, nerves, and connective tissues are affected by IRE ablation. However, because the tissue architecture remains intact, tissues are able to regenerate to some extent (2,3,5–9). One important focus of research into IRE is on imaging after ablation. The feasibility of detecting ablation zones by means of computed tomography (CT) has been reported in several preliminary animal studies (8–11).

Although CT is a widely used method for assessing the status after ablation, few data are available on CT imaging findings of ablation zones and treated tumors after IRE ablation in humans. The present study focuses on data of hepatic tumors and the surrounding liver parenchyma obtained by multislice spiral CT images

From the Department of Radiology (M.D., E.-M.J., L.B., C.N., R.M.-W., C.S., P.W.), University Hospital Regensburg, Franz-Josef-Strauß-Allee 11, 93042 Regensburg, Germany; and Institute of Diagnostic and Interventional Radiology (F.S.), Westküstenklinikum Heide, Heide, Germany. Received March 16, 2014; final revision received June 22, 2014; accepted June 24, 2014. **Address correspondence to** M.D.; E-mail: marco.dollinger@ukr.de

P.W. has a royalty agreement with AngioDynamics. None of the other authors have identified a conflict of interest.

J Vasc Interv Radiol 2014; 25:1589–1594

http://dx.doi.org/10.1016/j.jvir.2014.06.026

with an intravenous contrast agent 24–72 hours after percutaneous ablation by IRE and at midterm follow-up.

MATERIALS AND METHODS

Patients

In this study, 34 patients with 52 malignant nonresectable liver tumors ablated by IRE (number of procedures = 39) were retrospectively analyzed. The patient group consisted of 28 men (82.4%) and 6 women (17.6%) with a mean age of 64 years (range, 22–80 y). The cancer diagnoses of the patients are listed in Table 1. A solitary malignant liver tumor was present in 20 patients, and two to four hepatic malignancies (mean of 1.5 tumors per patient) were present in 14 patients. The largest diameter of the index lesion was 2.3 cm ± 1.2 (range, 0.5–6.3 cm).

Study Design and Participant Selection

A single-center retrospective observational study was conducted to assess and describe imaging findings after percutaneous IRE ablation of malignant liver tumors by means of contrast-enhanced CT scan. The study was approved by the local ethics committee. Each patient signed an informed consent form for the ablation procedure and the anonymous use of data for scientific purposes.

Before treatment, all patients were reviewed by members of an interdisciplinary tumor board who decided on the indication for IRE ablation. Patients were selected for IRE ablation if both surgical resection and thermal ablation were precluded. Exclusion criteria were presence of a cardiac defibrillator or pacemaker, coagulopathy, tumor resectability, unsuitability of the patient to undergo general anesthesia, or multifocal hepatic disease not amenable to complete ablation.

For this study, only the first IRE ablation of a hepatic tumor was evaluated. Patients with incomplete tumor ablation were excluded because the study design focused on the evolution of normal imaging results after complete ablation. The evaluation did not include any subsequent salvage IRE ablation procedures for recurrence of the previously treated tumor because prior therapy would disallow accurate assessment of the size or morphology of the ablation zone.

Table 1. Cancer Diagnoses in 34 Patients Treated with IRE of Malignant Liver Tumors

Diagnosis	No. Patients	No. Treated Lesions
Hepatocellular carcinoma	14	23
Colorectal tumor	11	16
Cholangiocellular carcinoma	5	7
Seminomatous testicular tumor	1	2
Esophageal carcinoma	1	1
Neuroendocrine tumor	1	2
Carcinoma of unknown primary origin	1	1
Total	34	52

IRE = irreversible electroporation.

Ablation Procedure

Ablation procedures were based on procedures described in previous studies (12,13). Imaging before the intervention was the basis for treatment planning. Using the size and shape of a tumor, the generator of the NanoKnife System (AngioDynamics, Latham, New York) calculated the position and number of electrodes for obtaining the required ablation zone, which included the treated tumor and an additional circumferential safety margin of 1 cm around the index tumor. Voltage was determined by a standard algorithm (AngioDynamics) using different factors, such as the intended area of the ablation zone, the distance between the probes, the number of probes, and the length of the active electrode tip (14).

In each patient, IRE ablation was carried out percutaneously using the NanoKnife System. The parameters of IRE ablation were 1,650–3,000 V, the pulse length was 90 μs, and 70 pulses were applied per cycle. All patients received a general anesthetic and a deep neuromuscular block.

Under CT fluoroscopy (CARE Vision, SOMATOM Sensation 16; Siemens Healthcare, Erlangen, Germany; CT parameters during fluoroscopy, tube voltage, 120 kVp; effective tube current-time product, 30 effective mAs; pitch 1; slice collimation, 16 mm × 0.75 mm), two to six monopolar 18-gauge ablation electrodes were placed parallel to each other, either around or into the target tumor. The target distance between the tips of the electrodes measured 0.7–2.0 cm. After verification of the correct position of the needles, a test pulse was delivered. After confirmation of adequate conductivity, therapeutic electrical impulses to the target tissue were applied that were automatically synchronized to the patient's cardiac cycle to prevent arrhythmia. The IRE electrodes were repositioned until complete ablation of the desired area.

Imaging Methods

Before ablation, all patients underwent a biphasic planning CT examination with a helical CT scanner (SOMATOM Sensation 16). Imaging during the intervention was carried out using CT fluoroscopy as described in the previous section. First imaging after the intervention (24–72 h after the ablation procedure) and follow-up imaging were conducted according to the standardized biphasic liver CT protocol to avoid complications and to assess the ablation status. CT parameters were as follows: tube voltage, 100 kVp (120 kVp in obese patients); effective tube current-time product, 160 effective mAs; slice collimation, 16 mm × 0.75 mm; pitch 1; slice thickness, 5 mm. CT images were obtained during the arterial phase using automatic bolus

triggering in the abdominal aorta at the level of the celiac trunk (CARE Bolus Software; Siemens Healthcare) about 25–40 seconds after the injection of intravenous contrast material. Images during the portal venous phase were acquired 75 seconds after contrast medium injection. Injection of 130 mL of a nonionic contrast medium (623 mg iopromide/mL; Ultravist 300; Schering AG, Berlin, Germany) at a rate of 3–4 mL/s was performed.

CT images were evaluated in a consensus reading by two radiologists with 8 years and 14 years of experience in abdominal imaging, respectively. The examiners evaluated the attenuation of the ablation defect, the presence and configuration of rim enhancement surrounding the ablation zone, the largest axial diameter, and the volume of the ablation defect as well as the presence of intralesional gas pockets. The attenuation of the ablation defect and the surrounding rim—if existent—was compared with the intact surrounding liver parenchyma. Volume and the largest axial diameter were semiautomatically determined by one of the two radiologists using the three-dimensional image processing program syngo.via with the MM Oncology package (Siemens Healthcare) during the portal venous phase. For determining volume and diameter, a rough diameter was drawn across the lesion in the axial plane. The software automatically drew a volume of interest around the contours of the ablation defect. Software assessments were checked by one of the radiologists and corrected manually, if necessary.

Statistical Analysis

Descriptive statistics were used to present results as absolute numbers (n), mean ± SD, and percentages. Data analysis was performed using Microsoft Office Excel 2003 (Microsoft Corporation, Redmond, Washington).

RESULTS

Computer-assisted measurements of the ablation zones on CT images obtained after ablation showed a mean maximum axial diameter of 5.9 cm ± 1.8 and an average volume of 57 mL ± 51. The follow-up CT examinations after an average period of 4.7 months showed a reduction in volume to 29% and in diameter to 61% of the initial values.

On early CT scans performed 24–72 hours after IRE treatment, ablated lesions were either homogeneously hypoattenuating (n = 36) or contained heterogeneously isoattenuating or hyperattenuating (n = 16) foci, or both, in a low-attenuation area. During the portal venous phase, isoattenuating and hyperattenuating foci showed similar enhancement of the contrast medium as during the arterial phase; in follow-up images, these foci were resolved. Peripheral contrast enhancement manifesting as a smooth delimited margin was observed during the arterial phase and the portal venous phase (Fig 1). Details are presented in Table 2.

Follow-up images were available for 36 ablation defects in 24 patients (mean follow-up, 4.7 mo; range, 0.3–17 mo). No evidence of peripheral contrast enhancement could be found during the arterial phase or during the portal venous phase.

On CT scans performed 24–72 hours after IRE ablation, gas pockets were documented in 38 of 52 (73.1%) ablation zones (Table 2) located both centrally and peripherally (Fig 2a–c). During a 30-day follow-up period, four patients developed clinical signs of infection on day 8, 8, 9, and 16 after IRE ablation. Because subsequent CT scans were suspicious for hepatic abscesses, each of the four patients underwent fluid aspirations that proved to be abscess formations in the ablation zones. Consequently, these patients received percutaneous drainage therapy and intravenous antimicrobial therapy. The follow-up CT images showed fully resorbed intralesional gas pockets in all lesions.

DISCUSSION

The advent of IRE, a novel nonthermal ablation technique, poses several challenges, such as the correct interpretation of images obtained shortly after IRE. Histologic examination of porcine livers within 24 hours after IRE ablation showed a sharp demarcation between the ablated zone and the adjacent unaffected paren-

Table 2. Numbers and Percentages of Hyperattenuating Rim Surrounding IRE Ablation Zone and of Intralesional Gas as Function of Acquisition Time of First CT Scan after IRE Ablation

Acquisition Time of CT after IRE Ablation (Day after Ablation Day)	No. Ablation Defects	Hyperattenuating Rim Surrounding Ablation Defect during					Intralesional Gas—No. Ablation Defects
		HAD Phase—No. Ablation Defects	PVD Phase—No. Ablation Defects	HAD and PVD Phase—No. Ablation Defects	HAD Phase Only—No. Ablation Defects	PVD Phase Only—No. Ablation Defects	
1	38	18 (47%)	26 (68%)	17 (45%)	1 (3%)	9 (23%)	29 (76%)
2	3	1 (33%)	3 (100%)	1 (33%)	0 (0)	2 (67%)	2 (67%)
3	11	4 (36%)	7 (64%)	4 (36 %)	0 (0)	3 (27%)	7 (64%)
Total	52	23 (44%)	36 (69%)	22 (42%)	1 (2%)	14 (27%)	38 (73%)

CT = computed tomography; HAD = hepatic arterial phase; IRE = irreversible electroporation; PVD = portal venous phase.

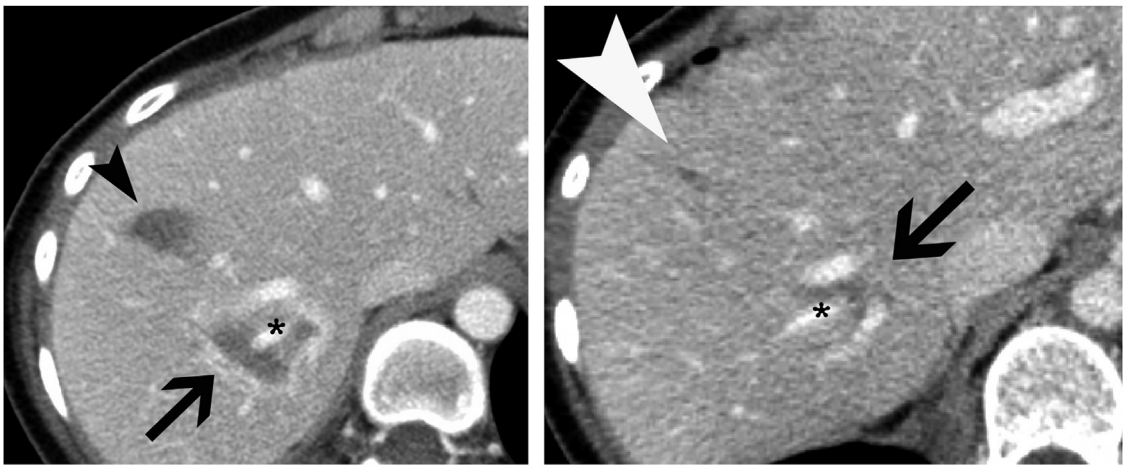

Figure 1. A 37-year-old woman underwent percutaneous ablation of two hepatic metastases of unknown origin. Within the same procedure, one metastasis was ablated by IRE, and the other metastasis was concurrently treated by RF ablation. Attenuation of ablation zones and the surrounding rim is determined compared with the surrounding liver parenchyma. **(a)** Contrast-enhanced CT scan of the liver during the portal venous phase performed 1 day after the IRE/RF ablation procedure shows two ablation zones: (*i*) a hypodense zone with clearly defined margins and surrounding regular contrast enhancement after IRE ablation (arrow) and (*ii*) a hypodense ablation area without any surrounding contrast enhancement after RF ablation (arrowhead). The asterisk indicates a perfused branch of the right hepatic vein. **(b)** Contrast-enhanced CT scan during the portal venous phase performed 2 months after the IRE/radiofrequency ablation procedure at the same level as **(a)** shows that peripheral enhancement has disappeared around the IRE ablation zone (arrow). The volume of the IRE ablation defect has decreased to approximately one third compared with the previous CT scan **(a)**. Only a partially imaged ablation defect is visible after RF ablation (arrowhead). The asterisk indicates a perfused branch of the right hepatic vein.

chyma (2,3,15). Shape and size of the ablation defects depend on the IRE parameters used and the type of tissue ablated (16,17). Histologic examination of the ablation defects showed cell death without any perivascular cellular sparing (2,3,8). This tissue necrosis was mainly due to apoptosis as indicated by immunohistochemical analysis (3,15). However, in some conditions, IRE ablation may lead to coagulation necrosis in perielectrode areas (18,19). Owing to vascular stasis, edematous, hyperemic, and inflammatory changes in ablated tissue and in the surrounding intact liver parenchyma were documented (2,3,9,16,18). Zhang et al (11) detected a decline in tumor cells of rodent livers 30 minutes after IRE ablation and loss of composition within 24 hours after ablation. Secondary to fibrotic changes, ablation defects decreased in a matter of weeks (2,18).

In preliminary animal studies, IRE ablation zones were described as low attenuating areas on unenhanced (11) as well as on contrast-enhanced CT images (9). Additionally, Lee et al (9) detected hyperintense foci within the ablation zones on contrast-enhanced CT images that were best seen during a delayed venous phase. In the present study, all patients showed hypoattenuating central ablation zones during the portal venous phase. This finding can be attributed to tissue necrosis caused by apoptosis shown by histopathologic examinations of porcine livers after IRE ablation (2,15). In 30.8% (16 of 52) of the ablation defects, isoattenuating or hyperattenuating foci, or both, were detected on CT images obtained 24–72 hours after the intervention. Previous in vitro studies have shown that identifying residuals or recurrences based solely on first follow-up images could be challenging, if not impossible (20). Lee et al (9) hypothesized that such focal hyperattenuations are probably caused by the release of contrast medium into the ablation defect secondary to an IRE-induced leakage of microvasculature within the defect zone. Because the foci in the present study were resolved on the follow-up CT images, they were probably caused by the presence of extraluminal contrast material or hemorrhage, or both. The presence of residual vital tumor tissue seems unlikely.

The hypodense ablation defects detected on contrast-enhanced CT images were surrounded by peripheral contrast enhancement in nearly 50% and 66% of cases during the arterial and portal venous phase, respectively. These findings, which were visible only on the first CT images after the intervention, are in line with the results after IRE ablation of porcine livers reported by Lee et al (3) and comparable to results described after radiofrequency ablation of hepatic tumors (21,22). Peripheral rim enhancement was visible in four of five (79.1%) lesions, indicating reactive hyperemia (21). The most probable explanation for rim enhancement in the present study is reactive hyperemia of edematous inflammatory origin adjacent to the ablation zone after IRE ablation, as supported by the results reported by Appelbaum et al (18) and Lee et al (3).

Another common finding on CT images obtained after intervention was gas accumulation within the ablation defects, which was evident in nearly three of four

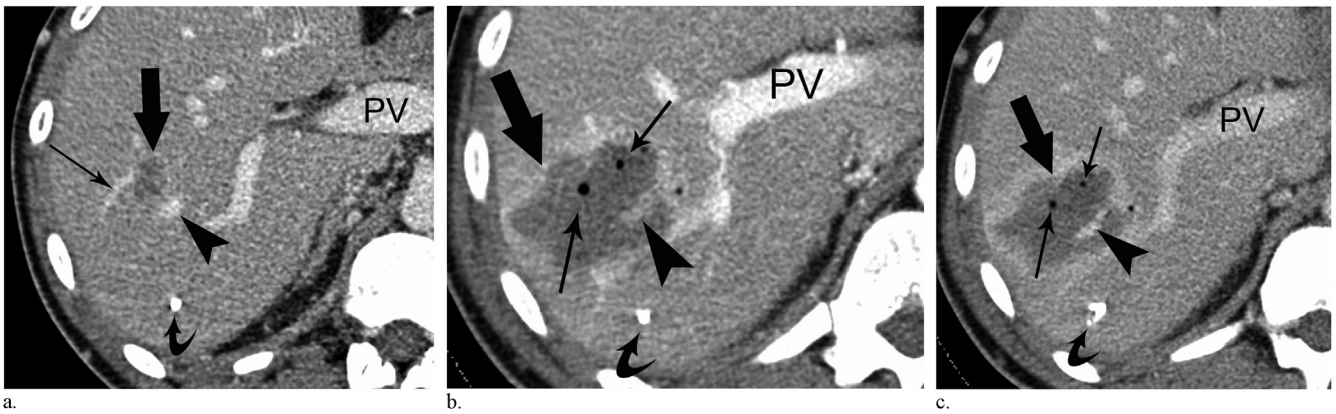

Figure 2. A 22-year-old man presented with a nonseminomatous testicular tumor and two hepatic metastases. **(a)** Intravenous contrast-enhanced portal venous phase image obtained 11 days before IRE ablation shows a hypodense lesion measuring 1.8 cm × 1.1 cm in segment V of the liver, correlating with a histologically confirmed metastasis of a nonseminomatous testicular tumor (thick arrow); this metastasis is located between a branch of the portal vein (thin arrow) and the right hepatic vein (arrowhead). The second metastasis is not shown in this layer. Surgical clip material after metastasectomy is indicated by the curved arrow (**a–c**). Intravenous contrast-enhanced arterial phase **(b)** and portal venous phase **(c)** images obtained 1 day after IRE ablation show a hypodense ablation zone (thick arrow) with peripheral enhancement in both phases. Note gas bubbles (thin arrows) within the lesion. The right hepatic vein (arrowhead) and the portal vein branch (not shown in this layer) are freely perfused without evidence of thrombosis. PV = portal vein.

ablation zones (73.1%). The incidence was higher than after RF ablation and microwave (MW) ablation with 62.8% and 18.9%, respectively (21,23). The analysis by Mitsuzaki et al (23) after MW ablation of 74 ablation zones in 63 patients yielded only 4 patients with intralesional gas pockets who subsequently developed an abscess. The clinical and paraclinical findings also indicated superinfection in each patient. Although gas formation during thermal ablation may have several causes, tissue boiling is the predominant one (24). Gas formation during IRE ablation is harder to explain; one possible explanation could be electrolysis of water caused by the high currents during IRE ablation, but no evidence is yet available.

Well-defined lesions with a central area of low attenuation surrounded by a peripheral rim of contrast enhancement with gas pockets—as found in the present study after IRE ablation during the portal venous phase—are also a characteristic feature of hepatic abscesses. The lesions are detected on dynamic CT scans in about 20% of cases (25). The similarity between the normal appearance of hepatic lesions after IRE ablation and typical descriptions of hepatic abscesses may limit the value of CT scanning for distinguishing normal changes after IRE ablation and pathologic changes. Laboratory results are essential in differentiating between normal findings after ablation and abscess formation, particularly because infections following IRE ablation have been reported (13).

As described in preliminary animal studies, the size of the ablation defect may decrease over weeks (2,10,18). In the present study, the hypoattenuating IRE ablation zones showed a volume reduction to less than one third (29%) of their initial volume on contrast-enhanced follow-up CT scans after a mean of 4.7 months. These findings are also in line with the results of Kingham et al (26), who reported rapid reduction of the ablation zones of liver tumors in humans after IRE treatment. This evolution of ablation defects is probably caused by fibrotic scarring (2,18).

These findings after IRE ablation need to be compared with CT findings after established thermal ablation procedures such as RF ablation and MW ablation. The low attenuation of ablation zone is similar to results after RF ablation (22,27,28) and MW ablation (23). A hyperattenuating rim surrounding the ablation defect is commonly found on CT images after intervention for each of the three ablation techniques, with an incidence of up to 92% after MW ablation (22,23,27,28). After MW ablation and RF ablation, this rim is expected to subside over time (22,23,27,28); this is in line with the CT findings at follow-up after IRE ablation. After IRE ablation, the incidence of intralesional gas bubbles is 73%—higher than after RF ablation (62.8%) (21) and MW ablation (18.9%) (23). However, in MW ablation, this finding was associated with abscess formation in 4 of 14 patients (23). Over the course of time, ablation defects decrease after RF ablation and MW ablation (21,23). After RF ablation, a volume reduction to about 80%, 50%, 35%, and 6% of the initial volume has been described after 1, 4, 7, and 19 months that may have been caused by fibrous and scar tissue (21).

This study has several limitations. The study group comprised a heterogeneous patient population with different tumor entities with primary and secondary hepatic tumors. No noncontrast CT phases were available that would have been helpful for enhancement measurement and for differentiating the cause of hyperattenuating rims surrounding the ablation defects and the isoattenuating and hyperattenuating foci within the ablation defects. However, to minimize radiation exposure, CT images were acquired only during the arterial and portal venous phases. Vascularity before imaging

and imaging results of the hepatic malignancies were not assessed. Another limitation is the lack of a long-term follow-up by means of CT scans and heterogeneous follow-up time points because the decision about obtaining such CT images was left to the discretion of the treating physician at the time.

In conclusion, the results of this study indicate that the normal CT appearance of hepatic lesions after IRE ablation may be very similar to the typical characteristics of hepatic abscesses. Consequently, careful analysis of such images and simultaneous consideration of clinical and paraclinical findings are required for distinguishing complications from normal changes after intervention.

ACKNOWLEDGMENT

The authors thank Dietlinde Ulsperger for editing the figures.

REFERENCES

1. Lee RC. Cell injury by electric forces. Ann N Y Acad Sci 2005; 1066:85–91.
2. Rubinsky B, Onik G, Mikus P. Irreversible electroporation: a new ablation modality—clinical implications. Technol Cancer Res Treat 2007; 6:37–48.
3. Lee EW, Chen C, Prieto VE, Dry SM, Loh CT, Kee ST. Advanced hepatic ablation technique for creating complete cell death: irreversible electroporation. Radiology 2010; 255:426–433.
4. Miller L, Leor J, Rubinsky B. Cancer cells ablation with irreversible electroporation. Technol Cancer Res Treat 2005; 4:699–705.
5. Deodhar A, Monette S, Single GW, et al. Renal tissue ablation with irreversible electroporation: preliminary results in a porcine model. Urology 2011; 77:754–760.
6. Schoellnast H, Monette S, Ezell PC, et al. Acute and subacute effects of irreversible electroporation on nerves: experimental study in a pig model. Radiology 2011; 260:421–427.
7. Li W, Fan Q, Ji Z, Qiu X, Li Z. The effects of irreversible electroporation (IRE) on nerves. PLoS One 2011; 6:e18831.
8. Lee YJ, Lu DSK, Osuagwu F, Lassman C. Irreversible electroporation in porcine liver: short- and long-term effect on the hepatic veins and adjacent tissue by CT with pathological correlation. Invest Radiol 2012; 47:671–675.
9. Lee YJ, Lu DSK, Osuagwu F, Lassman C. Irreversible electroporation in porcine liver: acute computed tomography appearance of ablation zone with histopathologic correlation. J Comput Assist Tomogr 2013; 37:154–158.
10. Lee EW, Wong D, Tafti BA, et al. Irreversible electroporation in eradication of rabbit VX2 liver tumor. J Vasc Interv Radiol 2012; 23:833–840.
11. Zhang Y, White SB, Nicolai JR, et al. Multimodality imaging to assess immediate response to irreversible electroporation in a rat liver tumor model. Radiology 2014; 271:721–729.
12. Silk MT, Wimmer T, Lee KS, et al. Percutaneous ablation of peribiliary tumors with irreversible electroporation. J Vasc Interv Radiol 2014; 25:112–118.
13. Philips P, Hays D, Martin RCG. Irreversible electroporation ablation (IRE) of unresectable soft tissue tumors: learning curve evaluation in the first 150 patients treated. PLoS One 2013; 8:e76260.
14. Thomson KR, Cheung W, Ellis SJ, et al. Investigation of the safety of irreversible electroporation in humans. J Vasc Interv Radiol 2011; 22:611–621.
15. Lee EW, Loh CT, Kee ST. Imaging guided percutaneous irreversible electroporation: ultrasound and immunohistological correlation. Technol Cancer Res Treat 2007; 6:287–294.
16. Ben-David E, Ahmed M, Faroja M, et al. Irreversible electroporation: treatment effect is susceptible to local environment and tissue properties. Radiology 2013; 269:738–747.
17. Appelbaum L, Ben-David E, Faroja M, Nissenbaum Y, Sosna J, Goldberg SN. Irreversible electroporation ablation: creation of large-volume ablation zones in in vivo porcine liver with four-electrode arrays. Radiology 2014; 270:416–424.
18. Appelbaum L, Ben-David E, Sosna J, Nissenbaum Y, Goldberg SN. US findings after irreversible electroporation ablation: radiologic-pathologic correlation. Radiology 2012; 262:117–125.
19. Faroja M, Ahmed M, Appelbaum L, et al. Irreversible electroporation ablation: is all the damage nonthermal? Radiology 2013; 266:462–470
20. Arena CB, Szot CS, Garcia PA, Rylander MN, Davalos RV. A three-dimensional in vitro tumor platform for modeling therapeutic irreversible electroporation. Biophys J 2012; 103:2033–2042.
21. Lim HK, Choi D, Lee WJ, et al. Hepatocellular carcinoma treated with percutaneous radio-frequency ablation: evaluation with follow-up multiphase helical CT. Radiology 2001; 221:447–454.
22. Dromain C, Baere T, de, Elias D, et al. Hepatic tumors treated with percutaneous radio-frequency ablation: CT and MR imaging follow-up. Radiology 2002; 223:255–262.
23. Mitsuzaki K, Yamashita Y, Nishiharu T, et al. CT appearance of hepatic tumors after microwave coagulation therapy. AJR Am J Roentgenol 1998; 171:1397–1403.
24. Chen W, Lafon C, Matula TJ, Vaezy S, Crum LA. Mechanisms of lesion formation in high intensity focused ultrasound therapy. Acoustics Research Letters Online 2003; 4:41–46.
25. Terrier F, Becker CD, Triller JK. Morphologic aspects of hepatic abscesses at computed tomography and ultrasound. Acta Radiol Diagn (Stockh) 1983; 24:129–137.
26. Kingham TP, Karkar AM, D'Angelica MI, et al. Ablation of perivascular hepatic malignant tumors with irreversible electroporation. J Am Coll Surg 2012; 215:379–387.
27. Lencioni R, Cioni D, Bartolozzi C. Percutaneous radiofrequency thermal ablation of liver malignancies: techniques, indications, imaging findings, and clinical results. Abdom Imaging 2001; 26:345–360.
28. Goldberg SN, Gazelle GS, Mueller PR. Thermal ablation therapy for focal malignancy: a unified approach to underlying principles, techniques, and diagnostic imaging guidance. AJR Am J Roentgenol 2000; 174:323–331.